Feasibility of Population-Based Input Function for Kinetic Modeling of [11C]-DPA-713

Mercy Iyabode Akerele (mercyoloniyo@yahoo.com)
Weill Cornell Medicine https://orcid.org/0000-0001-8856-8183

Sara Zein
Weill Cornell Medical College: Weill Cornell Medicine

Sneha Pandya
Weill Cornell Medical College: Weill Cornell Medicine

Anastasia Nikolopoulou
Weill Cornell Medical College: Weill Cornell Medicine

Susan A. Gauthier
Weill Cornell Medical College: Weill Cornell Medicine

Ashish Raj
Weill Cornell Medical College: Weill Cornell Medicine

Claire Henchcliffe
Weill Cornell Medical College: Weill Cornell Medicine

P. David Mozley
Weill Cornell Medical College: Weill Cornell Medicine

Nicolas A. Karakatsanis
Weill Cornell Medical College: Weill Cornell Medicine

Ajay Gupta
Weill Cornell Medical College: Weill Cornell Medicine

John Babich
Weill Cornell Medical College: Weill Cornell Medicine

Sadek A. Nehmeh
Weill Cornell Medical College: Weill Cornell Medicine

Original research

Keywords: population-based input function, kinetic modeling, [11C]DPA-713, normalization

Posted Date: November 19th, 2020

DOI: https://doi.org/10.21203/rs.3.rs-110221/v1

Feasibility of Population-Based Input Function for Kinetic Modeling of [^{11}C]-DPA-713

Mercy I. Akerele, PhD[a]; Sara A. Zein, PhD[a]; Sneha Pandya, MSc[a]; Anastasia Nikolopoulou, PhD[a]; Susan A. Gauthier, DO, MPH[a,b,c]; Ashish Raj, PhD[a]; Claire Henchcliffe, MD, DPhil[a,b]; P. David Mozley, MD[a]; Nicolas A. Karakatsanis, PhD[a]; Ajay Gupta, MD[a]; John Babich, PhD[a]; Sadek A. Nehmeh, PhD[a]

[a] Department of Radiology, Weill Cornell Medical College, New York, NY 10021

[b] Department of Neurology, Weill Cornell Medical College, New York, NY 10021

[c] Feil Family Brain and Mind Institute, Weill Cornell Medical College, New York, NY 10021

Corresponding Author

Mercy Akerele, Ph.D.

Department of Radiology, Weill Cornell Medical College, New York, NY 10021, USA.

E-mail: mia4006@med.cornell.edu

Tel.: +1(212)746-5552

Running title: PBIF-based [^{11}C]DPA-713 Kinetic Modeling

ABSTRACT

Introduction: Quantitative positron emission tomography (PET) studies of neurodegenerative diseases typically require the measurement of arterial input functions (AIF), an invasive and risky procedure. This study aims to assess the reproducibility of [^{11}C]DPA-713 PET kinetic analysis using population-based input function (PBIF). The final goal is to possibly eliminate the need for AIF.

Materials and Methods: Eighteen subjects including six healthy controls (HC) and twelve Parkinson disease (PD) subjects from two [^{11}C]-DPA-713 PET studies were included. Each subject underwent 90 minutes of dynamic PET imaging. Five healthy subjects underwent a test-retest scan within the same day to assess the repeatability of the kinetic parameters. Kinetic modeling was carried out using the Logan total volume of distribution (V_T) model. For each data set, kinetic analysis was performed using a patient specific AIF (PSAIF, ground-truth standard), and then repeated using the PBIF. PBIF was generated using the leave-one-out method for each subject from the remaining 17 subjects, and after normalizing the PSAIFs by 3 techniques: (a) $Weight_{subject} \times Dose_{Injected}$ (b) Area Under AIF Curve (AUC), and (c) $Weight_{subject} \times AUC$. The variability in the total distribution volume (V_T) measured with PSAIF, in the test/retest study were determined for selected brain regions (white matter, cerebellum, thalamus, caudate, putamen, pallidum, brainstem, hippocampus and amygdala) using the Bland-Altman analysis, and for each of the 3 normalization techniques. Similarly, for all subjects, the variabilities due to the use of PBIF were assessed.

Results: Bland-Altman analysis showed systematic bias between test and retest studies, which was reduced after normalizing the V_T estimate by the corresponding gray matter value. The corresponding mean bias and 95% limits of agreement (LOA) for the studied brain regions were 30% and 5%; ±70% and ±20% without and with gray matter normalization respectively.

Comparing PBIF- and PSAIF-based V_T estimate for all subjects and all brain regions, normalization by $Weight_{subject} \times AUC$ yielded the smallest 95% LOA among the three normalization techniques (±12%, ±13% and ±10% for $Weight_{subject} \times Dose_{Injected}$, AUC and $Weight_{subject} \times AUC$ respectively).

Conclusions: The variability in V_T is within that obtained for the test-retest studies. Therefore, V_T assessed using PBIF-based kinetic modeling is clinically feasible, and can be an alternative to PSAIF.

Keywords: population-based input function; kinetic modeling; [^{11}C]DPA-713; normalization

1. INTRODUCTION

18-kDa translocator protein (TSPO) receptor has been shown as a potential target for imaging neuroinflammation using PK-11195 PET (1–3). Recently, a putative antagonist of TSPO, [^{11}C]-N,N-diethyl-2[2-(4-methoxyphenyl)-5,7-dimethyl-pyrazolol[1,5-α]pyrimidin-3-yl]-acetamide ([^{11}C]DPA-713), was developed concurrently with the TSPO agonist, fluoro-ethoxy derivative [^{18}F]DPA-714.(4–6) Both [^{11}C]DPA-713 and [^{18}F]DPA-714 were shown to have higher affinity than the first generation TSPO tracer [^{11}C]-(R)-PK11195 (4,7,8). Several studies have now demonstrated the usefulness of [^{11}C]DPA-713 PET in quantifying neuroinflammation in different diseases, including multiple sclerosis (MS), Parkinson's disease (PD), and Alzheimer disease (AD), both in animal and human studies (4,9–12).

In PET, kinetic modeling is often essential for the accurate quantification of tracer uptake and metabolism in the tissue. This often requires the measurement of the tracer concentration in the arterial blood over time, an invasive and a potentially risky procedure(13), which can also adversely influence subject accrual (14).

An alternative technique such as an image-derived input function (IDIF) (15,16) or population-based input function (PBIF) (17,18) can facilitate the adoption of PET protocols requiring input functions. In brain studies, IDIF is usually deduced from the dynamic images of the carotid arteries, and hence is susceptible to partial volume effect (15–17). Previous studies showed the feasibility of PBIF as a robust alternative to IDIF for some radiopharmaceuticals (17,18). PBIF is generated by averaging the normalized patient-specific arterial input functions (PSAIFs) deduced from a cohort of subjects. Several normalization techniques have been reported in the literature; for example traditional scaling using blood samples by correlating the measured plasma activity with the AUC (17); correlation of the PBIF with PSAIF venous samples (19); scaling by injected dose and weight (20,21); and non-invasive scaling using individual parameters like weight, body surface area (BSA), and lean body mass (LBM) (17). Many studies have assessed the feasibility of PBIF for kinetic analysis using [^{18}F]FDG (18,22–25), yet very few studies involved neuroreceptor PET tracers (17,26), including TSPO brain studies (19,21,27). To the best of our knowledge, no PET kinetic modeling study has been performed with [^{11}C]DPA-713 using PBIF.

A major concern in the kinetic analysis of TSPO brain studies is the effect of genotype on the input functions. Owen *et al*. (28,29) demonstrated that the second generation TSPO tracers target two binding sites in humans, which leads to three affinity patterns: low-, high-, and mixed-affinity binders (LABs, HABs. and MABs, respectively). Past researches have shown that this variability in binding affinity has a major influence on the kinetic parameters where the values for HABs could be approximately twice that of MABs (29,30). Most studies therefore tend to carry out a genotype-based kinetic analysis for TSPO brain studies, especially when this involves any population-based implementation. However, for [^{11}C]-DPA-713 PET study, Coughlin et al (31) showed that different genotype- and physiological-related factors have varying degrees of influence on the global TSPO changes in the brain, thereby hindering accurate PET analysis, even among individuals with the same genotype. This was also confirmed by other TSPO studies (32–34). These previous studies also showed that normalization by the gray matter allows compensating for this genotypic dependency and other unknown physiological factors (not related to inflammation) that can affect the distribution of radiotracers binding to TSPO in the PET brain studies.

The aims of this study were to: (1) estimate the test-retest repeatability of the [^{11}C]DPA-713 PET imaging in healthy subjects, and (2) assess the reproducibility of kinetic analysis of [^{11}C]DPA-713 dynamic PET images of the brain with PBIF compared to PSAIF in healthy and PD subjects (based on the test-retest results). Kinetic parameters resulting from different PSAIF normalization techniques are also compared.

2. MATERIALS AND METHODS

A. Subjects

In total, twelve subjects (9 males and 3 females; age 56.6 ± 11.9 years) were recruited from a Parkinson's Disease (PD) dynamic [^{11}C]DPA-713 PET research study. Six additional healthy male subjects (age 42.6 ± 11.2 years) were also included, out of which five healthy subjects underwent test-retest studies to assess the repeatability of DPA kinetics. The inclusion criteria for the PD cohort are PD clinical diagnosis of 3 to 12 years of duration from onset of symptoms, age 30 to 70 years at time of enrollment, Hoehn and Yahr stage 2-3, and absence of a clinical diagnosis of dementia. Exclusion criteria included subjects receiving dopamine receptor blocking agents or treatment with acetylcholinesterase inhibitors; history of another significant neurological or major psychiatric disorder, or autoimmune disorders within the past 5 years.

B. PET Measurements and Reconstruction

PET data were acquired in list-mode format on a 4-ring Siemens Biograph mCT™ for a total of 90 minutes. The PET data were reconstructed into 32 dynamic frames (6×10 s, 4×30 s, 3×60 s, 2×120 s, 5×240 s, 12×300 s) using ordered subset expectation maximization (OSEM) with attenuation, scatter, and randoms corrections. Continuous arterial sampling was performed at 15 second intervals for the first 10 minutes using an automated fraction collector, followed by five additional samples collected at 20, 30, 45, 60, and 90 minutes respectively. Each of the blood samples was weighed and counted using a Wizard® automatic gamma counter (Perkin Elmer), and then the activity concentration was calculated. Blood samples drawn at 5, 10, 20, 30, 45, 60, and 90 minutes post-injection were also used to estimate metabolite fractions. The blood time activity curves (TACs) were finally corrected for metabolites, yielding a metabolite-corrected, arterial input function.

C. Data Analysis and Kinetic Modeling

Each subject underwent a T1-weighted MRI scan. Inter-frames head motion correction was achieved by rigidly co-registering the individual dynamic PET frames to the last 10 minutes imageset using PMOD (version 3.8; PMOD Technologies Ltd). The resulting dynamic imageset was then rigidly registered to the T1-MR imageset. Brain regions were delineated on the MRI images using FreeSurfer software (35), the corresponding Volumes of Interest (VOIs) were overlaid on the co-registered and motion-corrected dynamic PET images, and finally the corresponding TACs were deduced.

Kinetic modeling was done for each patient using the Logan V_T model. Kinetic analysis was performed using the PSAIFs, and then repeated using the PBIFs. For each of the selected brain structures (white matter, cerebellum, thalamus, caudate, putamen, pallidum, brainstem, hippocampus and amygdala), the total volume of distribution (V_T) were estimated with the blood volume fixed to 5%. Following the recommendations of past TSPO studies by Coughlin and others (31,33,36), the V_T was also normalized by the corresponding gray matter values (referred to as GM normalization in this study) to correct for physiologic factors (unrelated to inflammation) which may affect radioligand brain uptake (31,32,36). The gray matter was recommended for normalization because it is believed to have relatively uniform binding pattern in healthy participants (33).

D. Test-Retest Repeatability and Reliability

Five healthy control subjects underwent a test-retest within the same day to assess the reproducibility of the kinetic parameters in the brain structures. Kinetic analysis was carried out for all the selected brain regions, for both the test and retest datasets, using the Logan V_T model and the corresponding PSAIF's. The repeatability of V_T was assessed using the Bland-Altman analysis (37):

$$\%\ Relative\ Diff, D = \frac{Retest - Test}{(Retest + Test)/_2} \times 100 \quad (1)$$

$$Mean\ Bias = \frac{\sum_{n=1}^{N} D}{N} \quad (2)$$

The corresponding confidence interval of the mean bias (CI), 95% limits of agreement (LoA) and the coefficient of repeatability (CR) between test and retest were determined using:

$$LOA = Mean\ Bias \pm 1.96SD \quad (3)$$

$$CI_i = i \pm (t \times SE) \quad (4)$$

$$SE = \begin{cases} SD/\sqrt{N}, & for\ Bias \\ \sqrt{3SD^2/N}, & for\ LOA \end{cases} \quad (5)$$

where $N =$ number of subjects, and $i = Mean\ Bias,\ LOA$

$$CR = 1.96 \times \sqrt{\frac{\sigma^2}{N-1}} \quad (6)$$

where σ^2 is the variance of the relative difference, D, between the test and retest estimates. This represents the value below which the relative difference between test and retest is expected to lie with a 95% probability (37,38).

E. Generation of Population-Based Input Functions

The PBIFs were generated from the metabolic-corrected PSAIFs of all the 18 subjects under review. The individual PSAIFs were fitted using the "tri-exponential" function and then corrected for metabolites after fitting the later using "Watabe" function (as incorporated in PMOD). The metabolite-corrected PSAIFs for all subjects were interpolated to

the same time grid (with a step of 1 second) and then their peaks were aligned to the 30 second time-point where the majority of the IF peaks occurred. In order to reduce the influence of subject-induced variation on the generated PBIF, each of the metabolite-corrected PSAIFs was normalized by three methods: (a) $Weight_{subject} \times Dose_{Injected}$ (b) the corresponding AUC, and (c) $Weight_{subject} \times AUC$.

For each subject, PBIF was generated by averaging the normalized PSAIF of the other 17 subjects - leave-one-out procedure. (17,20,39,40) Individual subject IFs were then generated by appropriately scaling the PBIF with the corresponding factor, i.e. (a) $Weight_{subject} \times Dose_{Injected}$ (b) the corresponding AUC, and (c) $Weight_{subject} \times AUC$.

AUC scaling was done by tail-fitting the PBIF and the PSAIF using the last 30 minutes time points as this best reproduced the actual subject AUC. The reproducibility of V_T using PBIF was assessed using Bland-Altman analysis, with PSAIF values as gold reference. For each structure, the % relative difference (Relative Diff), D, between the parameters was estimated using:

$$\%\ Relative\ Diff,\ D = \frac{P_{PBIF} - P_{PSAIF}}{P_{PSAIF}} \times 100 \quad (7)$$

where P_{PBIF} and P_{PSAIF} are the kinetic parameters generated by PBIF and PSAIF respectively.

The bias, upper and lower limits of agreements (LoA), and the corresponding 95% confidence intervals (CI) were estimated using equations (2-5).

F. Statistical Analysis

Data were analyzed using SPSS (IBM SPSS statistics for windows, version 26.0) and Real statistics (http://www.real-statistics.com/) software. Normality of distribution was tested using the Shapiro-Wilk test. The statistical difference between the three normalization techniques was evaluated using the one-way Analysis of Variance (ANOVA). The pairwise t-test was also performed as a follow-up test to ANOVA in order to reveal which specific pair of the normalization techniques are significantly different, and Bonferroni correction was applied to correct for the potential error due to multiple testing. In all cases, a P-value < 0.05 was considered to suggest statistical significance.

3. RESULTS

A. Test-Retest Repeatability and Reliability

The repeatability of the V_T estimates for all selected brain regions of interest in the test-retest studies are shown in Figure 1, and results are displayed without and with GM Normalization.

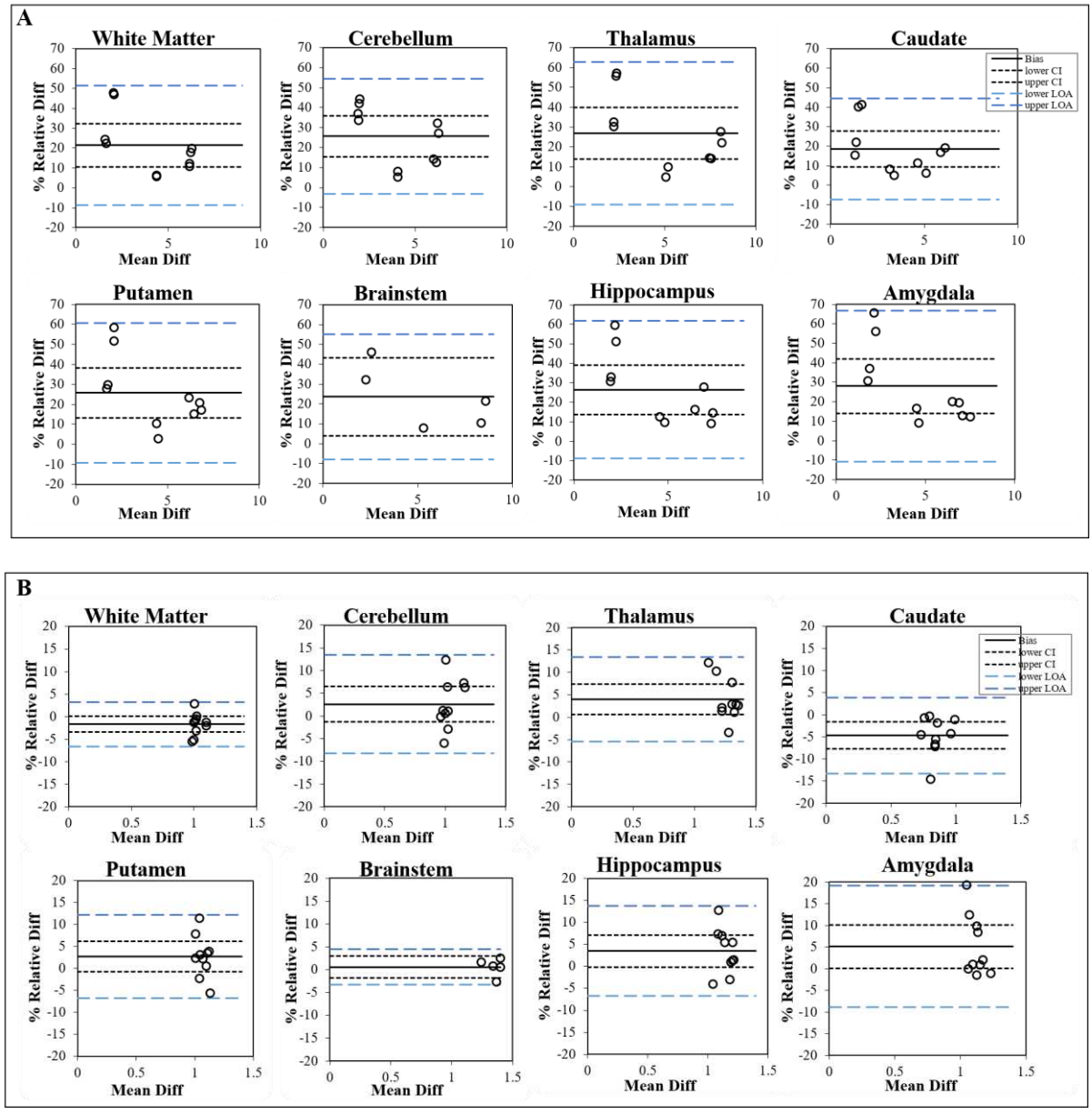

Figure 1 *Bland-Altman plot comparing the test-retest repeatability of Vt estimates for all selected brain regions of interest: (A) without GM normalization and (B) with GM normalization respectively. The solid line is the mean % bias between test and retest V_T estimate, while the doted and dashed lines represent the %CI and %LOA respectively*

Without GM normalization, the V_T estimates in the retest studies exhibited positive bias (ranging from 20 to 30%) compared to those deduced from the test studies (Figure 1A), where all the differences lie above the zero line (systematic bias). This systematic bias between test and retest V_T estimates was compensated for after normalization by the corresponding values of the GM resulting in a bias within ±5% for all brain regions (Figure 1B). The LOA also reduced with GM normalization (from ~70% to ~20%).

Normalization by the GM also resulted in reducing both the % bias and CR between the test and retest kinetic parameters. The corresponding results with and without normalization by the GM are summarized in Figure 2 and Table 1. V_T values exhibited a large reduction in the mean % bias between test and retest studies after normalization by the corresponding GM values (from ~30% to ~5%). The V_T values also showed improved CR after GM normalization (from ~15% to ~5%) (Figure 2B). Based on the advantage of normalizing the V_T by the corresponding GM values to remove systematic bias and improve repeatability as outlined above, all the remaining analysis in this work has been reported with and without GM normalization.

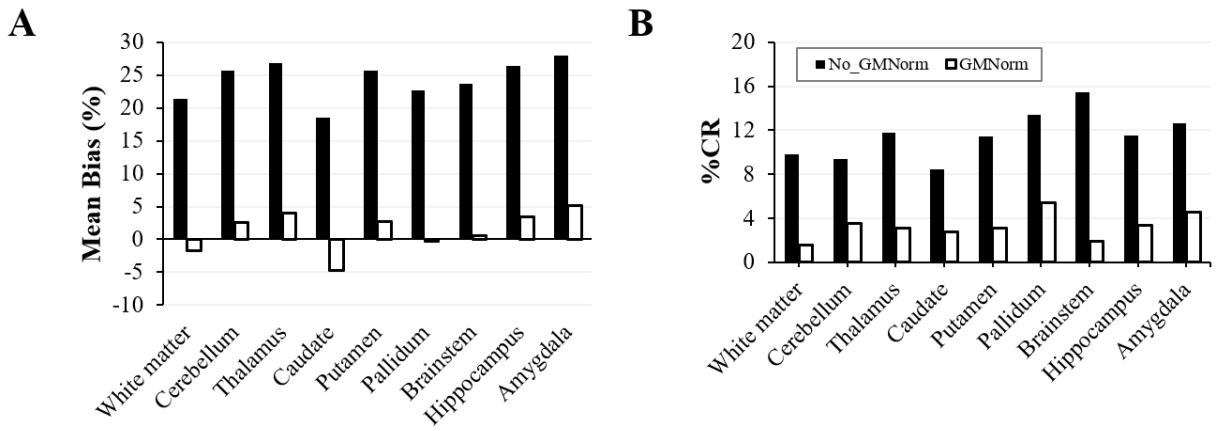

Figure 2 *Effect of GM normalization on the (a) mean % bias and (b) CR of the test-retest V_T estimate*

Table 1 shows the repeatability of the test-retest for the 5 healthy subjects as estimated by the Bland-Altman analysis (equations (1-5)). With GM normalization, V_T exhibited reduced variability between the test and retest studies (95% LOA reduced from ±70% to ±20%) for all the brain regions.

Table 1 *Bland-Altman analysis of the variation in* V_T *estimates between the test and retest*

	Regions	Test Mean	Retest Mean	Mean % bias ± SD	95% CI	95% LoA
Without GM normalization	White matter	3.74 ± 2.02	4.43 ± 2.14	21.43 ± 15.08	10.64 to 32.22	-8.74 to 51.60
	Cerebellum	3.61 ± 1.87	4.50 ± 2.15	25.69 ± 14.40	15.38 to 35.99	-3.12 to 54.50
	Thalamus	4.51 ± 2.50	5.61 ± 2.77	26.89 ± 18.01	14.01 to 39.77	-9.12 to 62.90
	Caudate	3.16 ± 1.84	3.68 ± 2.02	18.52 ± 12.94	9.26 to 27.78	-7.36 to 44.40
	Putamen	3.83 ± 2.12	4.71 ± 2.31	25.71 ± 17.47	13.21 to 38.21	-9.24 to 60.65
	Pallidum	4.06 ± 2.24	4.83 ± 2.35	22.70 ± 20.56	7.99 to 37.41	-18.41 to 63.82
	Brainstem	4.91 ± 2.92	5.92 ± 3.15	23.61 ± 15.80	3.99 to 43.23	-7.99 to 55.21
	Hippocampus	4.09 ± 2.29	5.04 ± 2.39	26.44 ± 17.65	13.82 to 39.06	-8.85 to 61.73
	Amygdala	4.04 ± 2.35	4.99 ± 2.42	27.98 ± 19.40	14.11 to 41.86	-10.81 to 66.78
With GM normalization	White matter	1.03 ± 0.04	1.02 ± 0.04	-1.69 ± 2.45	-3.45 to 0.06	-6.50 to 3.11
	Cerebellum	1.02 ± 0.06	1.05 ± 0.09	2.61 ± 5.42	-1.27 to 6.48	-8.01 to 13.23
	Thalamus	1.24 ± 0.10	1.29 ± 0.07	3.95 ± 4.71	0.57 to 7.32	-5.29 to 13.18
	Caudate	0.86 ± 0.08	0.82 ± 0.08	-4.68 ± 4.29	-7.75 to -1.61	-13.09 to 3.72
	Putamen	1.05 ± 0.06	1.08 ± 0.04	2.72 ± 4.77	-0.69 to 6.14	-6.62 to 12.07
	Pallidum	1.12 ± 0.06	1.11 ± 0.06	-0.29 ± 8.28	-6.21 to 5.64	-16.52 to 15.95
	Brainstem	1.35 ± 0.07	1.35 ± 0.06	0.57 ± 1.93	-1.83 to 2.97	-3.22 to 4.36
	Hippocampus	1.13 ± 0.07	1.17 ± 0.06	3.48 ± 5.11	-0.18 to 7.13	-6.55 to 13.50
	Amygdala	1.09 ± 0.08	1.15 ± 0.05	5.12 ± 6.99	0.12 to 10.13	-8.58 to 18.83

B. Evaluation of the PBIF and the Normalization Criteria

The PBIF was generated using the PSAIF of all eighteen subjects included in this study. Figure 3 shows the overlaid normalized PSAIFs (Figure 3A) and the resulting PBIF generated after normalizing each PSAIF by $\text{Weight}_{\text{subject}} \times \text{AUC}$ (Figure 3B).

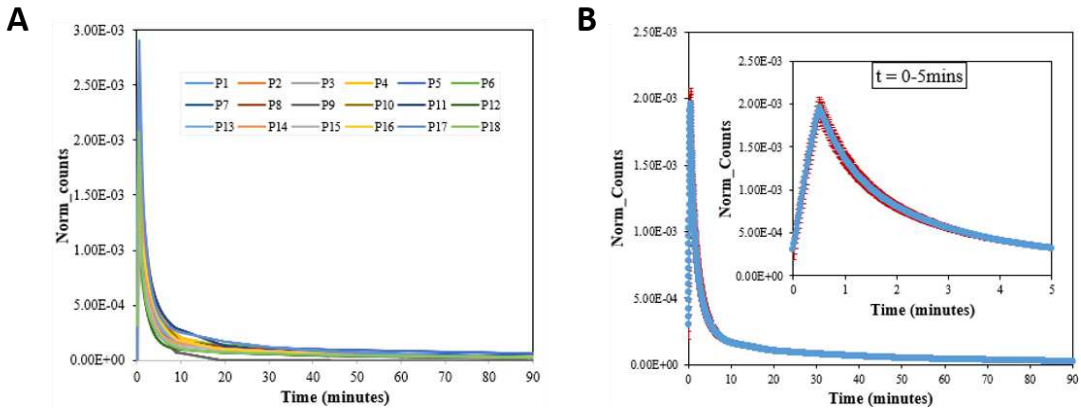

Figure 3 *Overlaid normalized PSAIFs from all 18 patients (A) and the resulting PBIF generated by normalization with* $\text{Weight}_{\text{subject}} \times \text{AUC}$ *(B). The zoomed PBIF over the first 5 minutes is also shown. In (b), the blue points are the mean PBIF while the red points are the standard error of the mean (SEM)*

Figure 4 shows the % difference and the LoAs between the V_T estimates generated by the PSAIF and PBIF for selected brain regions. The comparison is made using PSAIF and the PBIF generated by the three normalization techniques.

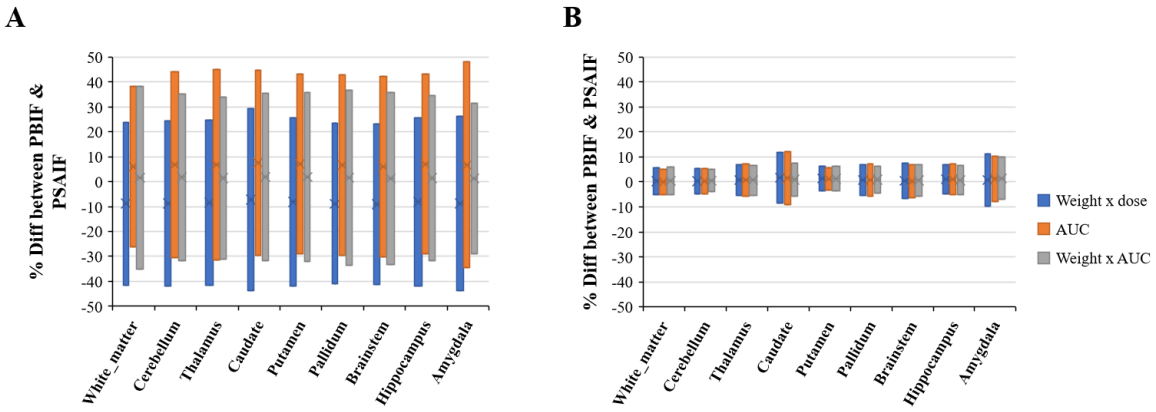

Figure 4 *The % relative difference in V_T and the LoAs between PSAIF and PBIF of some specific structures as generated by the three normalization techniques: (A) without GM normalization, (B) with GM normalization*

Without GM normalization, the mean % difference is -10% for $Weight_{subject}$×$Dose_{Injected}$; +8% for AUC and +2% for $Weight_{subject}$×AUC; while the LoAs lie within ±45% for $Weight_{subject}$×$Dose_{Injected}$; ±50% for AUC and ±35% for $Weight_{subject}$×AUC. The ANOVA analysis shows a significant difference between the results generated by the three normalization techniques for all brain structures except the brainstem (*P*-value = 0.095). Although for the same brainstem, the pairwise test shows a significant difference between $Weight_{subject}$×$Dose_{Injected}$ versus AUC (*P*-value = 0.034). However, with GM normalization, no statistically significant differences (*P*-value > 0.05) existed in the % difference among the three normalization techniques. The three normalization techniques, however, yielded slight differences for the LoAs measurements: (LoAs lie within ±12% for $Weight_{subject}$×$Dose_{Injected}$; ±13% for AUC and ±10% for $Weight_{subject}$×AUC). In all cases, normalizing by $Weight_{subject}$×AUC yielded the smallest % bias and variability (% bias = ±2% and ±1.5%; LOA = ±38% and ±10% without and with GM normalization respectively) for all brain regions.

The mean bias (±SD) between the PSAIF and PBIF for the V_T generated by normalization with $Weight_{subject}$×AUC are shown in Figure 5 and Table 2 (for all brain regions).

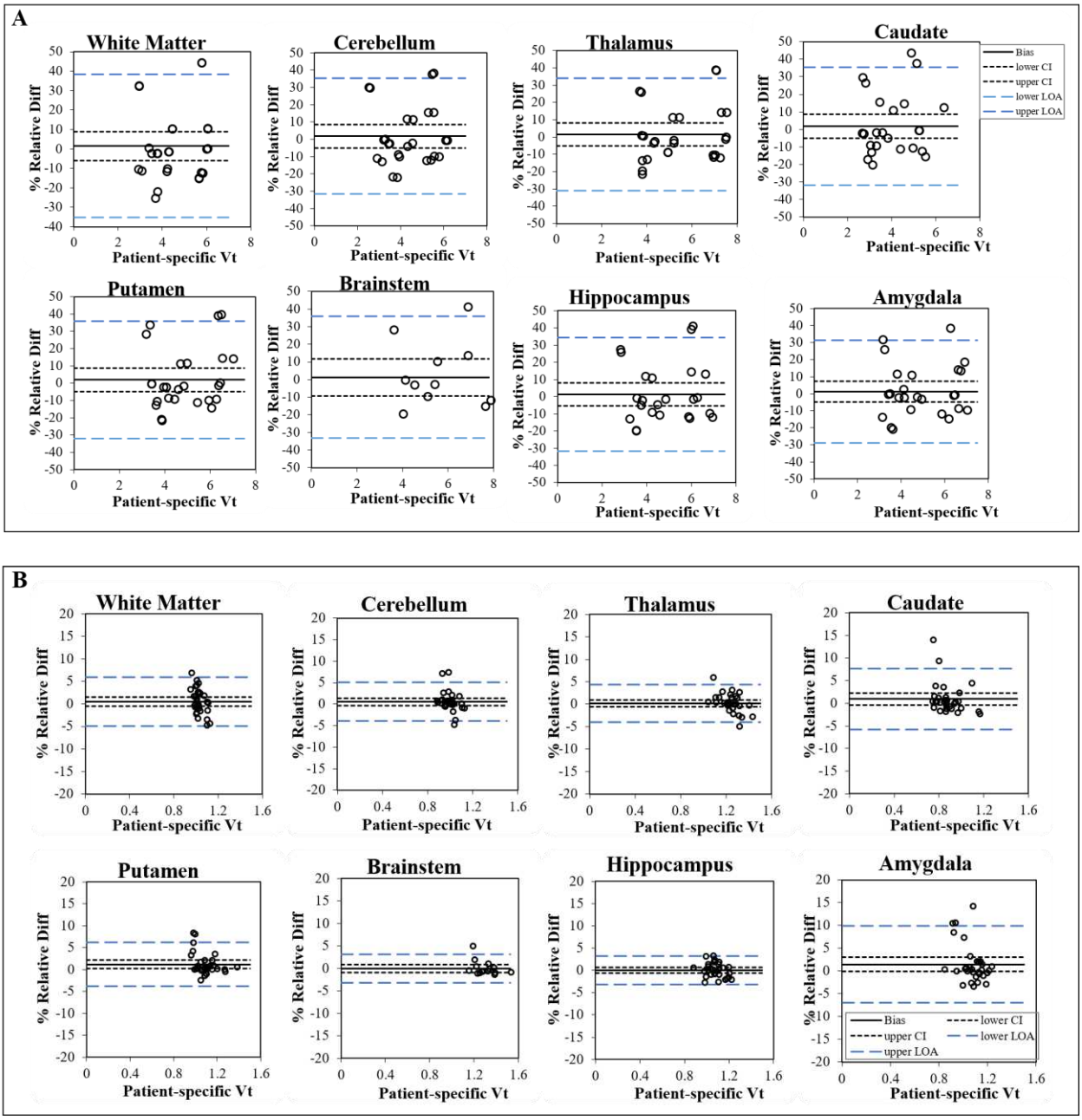

Figure 5 *Bland-Altman analysis showing the variation in the V_T between the PSAIF and PBIF (normalization with* $Weight_{subject} \times AUC$*) with (A) no GM normalization and (B) GM normalization. The solid line is the mean % bias between PSAIF and PBIF V_T estimate, while the doted and dashed lines represent the %CI and %LOA respectively*

Without GM normalization, the mean bias for V_T lies within ±2%, with amygdala showing the smallest (1.21%) deviation, and putamen showing the highest (1.91%). With GM normalization, the mean bias for V_T lies within ±1.5%,

with brainstem showing the smallest (-0.02%) deviation, and putamen showing the highest (1.20%). Overall, the 95% LoA for all brain regions lies within ±38% and ±10% without and with GM normalization respectively.

Table 2 *Bland-Altman analysis of the variation in V_T estimate between the PSAIF and PBIF (normalization with* $Weight_{subject} \times AUC$*)*

Regions	Without GM normalization			With GM normalization		
	Mean % bias ± SD	95% CI	95% LoA	Mean % bias ± SD	95% CI	95% LoA
White matter	1.51 ± 18.74	-6.06 to 9.07	-35.22 to 38.23	0.48 ± 2.78	-0.53 to 1.48	-4.98 to 5.93
Cerebellum	1.73 ± 17.09	-5.17 to 8.63	-31.75 to 35.22	0.51 ± 2.30	-0.32 to 1.34	-0.63 to 2.24
Thalamus	1.45 ± 16.57	-5.24 to 8.14	-31.02 to 33.93	0.18 ± 2.13	-0.62 to 0.97	-3.99 to 4.35
Caudate	1.80 ± 17.14	-5.12 to 8.73	-31.79 to 35.40	0.93 ± 3.43	-0.35 to 2.21	-5.80 to 7.66
Putamen	1.91 ± 17.27	-5.07 to 8.89	-31.96 to 35.77	1.20 ± 2.57	0.25 to 2.16	-3.82 to 6.23
Pallidum	1.57 ± 17.95	-5.67 to 8.82	-33.60 to 36.75	0.49 ± 1.86	-0.21 to 1.18	-3.16 to 4.13
Brainstem	1.28 ± 17.67	-9.39 to 11.96	-33.35 to 35.92	-0.02 ± 1.63	-0.92 to 0.89	-3.22 to 3.18
Hippocampus	1.36 ± 16.86	-5.44 to 8.18	-31.67 to 34.41	0.03 ± 1.64	-0.58 to 0.64	-3.18 to 3.24
Amygdala	1.21 ± 15.42	-5.01 to 7.45	-29.01 to 31.45	1.45 ± 4.28	-0.12 to3.01	-6.95 to 9.84

4. DISCUSSION

Several studies have shown the feasibility to image neuroinflammation in multiple sclerosis (MS), Parkinson's disease (PD), and Alzheimer disease (AD) using [^{11}C]DPA-713 PET for quantifying differences between patients and controls (4,9–12). Accurate quantification of tracer uptake and metabolism in the tissue through kinetic modeling often requires blood sampling,(13) or some alternative approach such as simplified reference modeling (41,42), cluster analysis (41,43) or image-derived input function (IDIF) techniques. The apparent limitations of these approaches (15–17,19,21,44) are giving way to the exploration of the population-based input function (PBIF) approach as a more quantitatively reliable and less invasive alternative.

In this study, we have assessed the reproducibility of kinetic analysis of [^{11}C]DPA-713 dynamic PET images using PBIF, compared to PSAIF, in a cohort of subjects with Parkinson Disease. The repeatability of the V_T estimate was also assessed in a cohort of healthy subjects that underwent a test-retest [^{11}C]DPA-713 dynamic PET within the same day. Kinetic analysis with PSAIF was determined to be reproducible with PBIF if the corresponding LoA are within those of the test-retest study.

The test-retest repeatability of the [^{11}C]DPA-713 uptake exhibited systematic increase in uptake values between test and retest (Figure 1). Although the cause of this bias is yet to be fully explored because most repeatability studies are done days or even weeks apart (34). Few recent studies that performed same day retest have reported the same systematic bias, and they suggested that the possible explanation to this systematic bias could be due to hormone-mediated changes in TSPO expression, tonic changes due to scan-related stress/anxiety, or alteration in blood cholesterol due to food intake between the test and retest scans (45,46). While performing the test and retest studies under similar conditions on different days could eliminate this bias, other parameters such as alteration in TSPO density due to chronic disease as well as non-disease-related factors may be difficult to control (31). Owen *et al.* (28,29) demonstrated that the second generation TSPO tracers target two binding sites in humans, which leads to three affinity patterns: low-, high-, and mixed-affinity binders (LABs, HABs. and MABs, respectively). Past researches have shown that this variability in binding affinity has a major influence on the kinetic parameters where the values for HABs could be approximately twice that of MABs (29,30). For [^{11}C]-DPA-713 dynamic PET studies, Coughlin *et al.* (31) argued that those genotype- as well as other unknown physiological factors have varying degrees of influence on the global TSPO changes in the brain, thereby hindering accurate PET analysis, even among individuals with the same genotype. He therefore stated that the dependencies of the kinetic parameters can be compensated for by normalizing them with the corresponding GM parameters kinetic rate constants. This was confirmed in other TSPO studies (32–34), and adopted in here.

One potential approach to compensate for the bias between the test and retest studies is by normalization by the corresponding kinetic parameters of the GM as suggested by past studies (31,36) and also shown by this study. Without GM normalization, the % relative difference between test and retest V_T values lies significantly above the zero line for all structures, indicating that retest values are always higher than test values. But with GM normalization,

the % relative difference is symmetric about the zero line. The mean % Diff and the LOA are also significantly reduced, thereby improving repeatability. The detailed results are presented in Figures 1 and 2 where the average percent biases over all brain regions were reduced from 30% to 5% after normalization. Normalization by the GM also resulted in improving the repeatability of kinetic analysis (the LOA changes from 70% to 20%; and the CR reduced from 15% to 5%).

Ye *et al.* (47) opined that the bias in kinetic parameter estimation in direct reconstruction with PBIF depends on the normalization and scaling technique used. In this study, we have assessed and compared three normalization approaches: (a) $Weight_{subject} \times Dose_{Injected}$, (b) AUC, and (c) $Weight_{subject} \times AUC$. An example of the normalized PSIFs and the resulting PBIF are shown in Figure 3. The performance of these techniques was evaluated using the percent relative difference between the PSAIF- and PBIF- derived V_T in selected brain regions (Figure 4). Without GM normalization, there is a significant difference between the three normalization techniques for all brain structures except the brainstem, but with GM normalization, no statistically significant differences among those three techniques were observed.

Several normalization techniques have been reported in the literature which include: traditional scaling using blood samples by correlating the measured plasma activity at a given time-point with the AUC;(17) correlation of the PBIF with AIF at any time-point using venous samples (19); by accounting for injected dose and weight (20,21); non-invasive scaling using individual parameters like weight, body surface area (BSA), and lean body mass (LBM) (17). In this study, we have assessed the three aforementioned normalization approaches. Subsequently, a subject IF was deduced by scaling the PBIF by his/her weight and injected dose. In the case of AUC normalization, that was measured after scaling the PBIF by the ratio of the average activity concentration of blood samples acquired over the last 30 minutes of the dynamic scan and that of the tail of the PBIF over the same time frames (this setting was used as this best predicted the original subject AUC; result not shown). Practically, venous blood samples may be used instead for scaling purpose assuming that arterial and venous blood reach equilibrium at about 30-45 minutes post-injection time (17). In this study, normalization by $Weight_{subject} \times AUC$ yielded the smallest % bias (±2%) and variability (LoAs ±38%) between PBIF and PSAIF. Furthermore, the LOA of the V_T estimates (either without or with GM normalization) were within those of the repeatability study (determined from the test/retest) (Table 1), thus the

corresponding PBIF can be an alternative for PSAIF for kinetic modeling of [^{11}C]DPA-713 dynamic PET images of the brain.

V_T measured with PBIF showed good reproducibility (LOA of ±38% and ±10%) but with a positive bias (±2% and ±1.5%) without and with GM normalization respectively (Figure 5 and Table 2). These were also in agreement with the findings of Lavisse *et al.* (19) As a final note, the reproducibility of the PBIF-based V_T estimates compared with PSAIF-based V_T fall well within the test-retest results, either with, or without GM normalization, hence showing the feasibility of [^{11}C]-DPA-713 PET kinetic modelling using PBIF.

A major limitation for this study is the relatively small sample size (n = 18), even though our findings are in agreement with previous results of smaller (n = 9) (19) and larger (n = 42) (20) sample sizes. The common thing is that these studies normalize the individual input functions to remove variabilities in the PBIF. This might suggest that the efficiency of the PBIF in accurately estimating the kinetic parameters depend less on the sample size used, but more on the normalization. This was also consolidated by Ye *et al*. (47) who opined that the bias in kinetic parameter estimation in direct reconstruction with PBIF was mostly due to inaccuracy in normalization and scaling.

CONCLUSION

This study demonstrated the feasibility of [^{11}C]-DPA-713 PET kinetic modelling using PBIF, thus potentially alleviating the need for arterial blood sampling. Moreover, it was shown that the optimal result in terms of kinetic parameter accuracy was obtained when the PSAIFs were normalized with $Weight_{subject} \times AUC$. Finally, V_T showed more reproducibility after normalizing the targeted kinetic parameter to those estimated in gray matter. However, this does not in any way affect the feasibility of using PBIF as an alternative to PSAIF for [^{11}C]-DPA-713 PET kinetic analysis as reflected in this study.

COMPLIANCE WITH ETHICAL STANDARDS

Funding: This study was funded by the National Center for Advancing Translational Sciences of the National Institutes of Health under Award Numbers UL1TR000457 and RO1 NS104283.

Conflict of Interest: All authors have no relevant financial or non-financial conflicts of interest to disclose.

Ethical Approval: All procedures performed in the human studies contained in this work were in accordance with the ethical standards of the institutional review board at the Weill Cornell Medical College, New York, USA.

Informed Consent: Informed consent was obtained from all individual participants included in this study.

REFERENCES

1. Cumming P, Burgher B, Patkar O, Breakspear M, Vasdev N, Thomas P, et al. Sifting through the surfeit of neuroinflammation tracers. J Cereb Blood Flow Metab. 2018;38(2):204–24.

2. Hagens M, Berckel B, Barkhof F. Novel MRI and PET markers of neuroinflammation in multiple sclerosis. Curr Opin Neurol. 2016;29(3):229–36.

3. Airas L, Rissanen E, Rinne J. Imaging of microglial activation in MS using PET: Research use and potential future clinical application. Mult Scler. 2017;23(4):496–504.

4. Boutin H, Chauveau F, Thominiaux C, Gregoire MC, James ML, Trebossen R, et al. C-11-DPA-713: A novel peripheral benzodiazepine receptor PET ligand for in vivo imaging of neuroinflammation. J Nucl Med. 2007;48(4):573–81.

5. Fookes CJR, Pham TQ, Mattner F, Greguric I, Loc'h C, Liu X, et al. Synthesis and biological evaluation of substituted F-18 imidazo 1,2-a pyridines and F-18 pyrazolo 1,5-a pyrimidines for the study of the peripheral benzodiazepine receptor using positron emission tomography. J Med Chem. 2008;51(13):3700–12.

6. Kreisl WC, Fujita M, Fujimura Y, Kimura N, Jenko KJ, Kannan P, et al. Comparison of [(11)C]-(R)-PK 11195 and [(11)C]PBR28, two radioligands for translocator protein (18 kDa) in human and monkey: Implications for positron emission tomographic imaging of this inflammation biomarker. Neuroimage. 2010;49(4):2924–32.

7. James ML, Fulton RR, Vercoullie J, Henderson DJ, Garreau L, Chalon S, et al. DPA-714, a new translocator protein-specific ligand: synthesis, radiofluorination, and pharmacologic characterization. J Nucl Med. 2008;49(5):814–22.

8. Endres CJ, Pomper MG, James M, Uzuner O, Hammoud DA, Watkins CC, et al. Initial Evaluation of C-11-DPA-713, a Novel TSPO PET Ligand, in Humans. J Nucl Med. 2009;50(8):1276–82.

9. Doorduin J, Klein HC, Dierckx RA, James M, Kassiou M, de Vries EFJ. C-11 -DPA-713 and F-18 -DPA-714 as New PET Tracers for TSPO: A Comparison with C-11 -(R)-PK11195 in a Rat Model of Herpes Encephalitis. Mol Imaging Biol. 2009;11(6):386–98.

10. Rosenberg P, Endres C, Lyketsos C, Coughlin J, Kassiou M, Pomper M. Quantifying translocator protein (TSPO) in Alzheimer's disease and cognitively healthy older persons with 11C-DPA-713 PET imaging. Alzheimer's Dement. 2011;7:S725–S725.

11. Zimmer ER, Leuzy A, Benedet AL, Breitner J, Gauthier S, Rosa-Neto P. Tracking neuroinflammation in Alzheimer's disease: the role of positron emission tomography imaging. J Neuroinflammation. 2014;11:120.

12. Terada T, Yokokura M, Yoshikawa E, Futatsubashi M, Kono S, Konishi T, et al. Extrastriatal spreading of microglial activation in Parkinson's disease: a positron emission tomography study. Ann Nucl Med. 2016;30(8):579–87.

13. Bentourika M. Kinetic modeling of PET-FDG in the brain without blood sampling. Comput Med Imaging Graph. 2006;30(8):447–51.

14. Kang Y, Mozley PD, Verma A, Schlyer D, Henchcliffe C, Gauthier SA, et al. Noninvasive PK11195-PET Image Analysis Techniques Can Detect Abnormal Cerebral Microglial Activation in Parkinson's Disease. J Neuroimaging. 2018 Sep 1;28(5):496–505.

15. Watabe H, Channing MA, Riddell C, Jousse F, Libutti SK, Carrasquillo JA, et al. Noninvasive estimation of the aorta input function for measurement of tumor blood flow with. IEEE Trans Med Imaging. 2001;20(3):164–74.

16. Mourik JEM, van Velden FHP, Lubberink M, Kloet RW, van Berckel BNM, Lammertsma AA, et al. Image derived input functions for dynamic High Resolution Research Tomograph PET brain studies. Neuroimage. 2008;43(4):676–86.

17. Zanotti-Fregonara P, Hines CS, Zoghbi SS, Liow JS, Zhang Y, Pike VW, et al. Population-based input

function and image-derived input function for C-11 (R)-rolipram PET imaging: Methodology, validation and application to the study of major depressive disorder. Neuroimage. 2012;63(3):1532–41.

18. Brock CS, Young H, Osman S, Luthra SK, Jones T, Price PM. Glucose metabolism in brain tumours can be estimated using [18F] 2-fluorodeoxyglucose positron emission tomography and a population-derived input function scaled using a single arterialised venous blood sample. Int J Oncol. 2005;26(5):1377–83.

19. Lavisse S, Garcia-Lorenzo D, Peyronneau MA, Bodini B, Thiriez C, Kuhnast B, et al. Optimized quantification of translocator protein radioligand F-18-DPA-714 uptake in the brain of genotyped healthy volunteers. J Nucl Med. 2015;56(7):1048–54.

20. Zanotti-Fregonara P, Hirvonen J, Lyoo CH, Zoghbi SS, Rallis-Frutos D, Huestis MA, et al. Population-Based Input Function Modeling for F-18 FMPEP-d(2), an Inverse Agonist Radioligand for Cannabinoid CB1 Receptors: Validation in Clinical Studies. PLoS One. 2013;8(4):e60231.

21. MacAskill MG, Walton T, Williams L, Morgan TEF, Alcaide-Corral CJ, Dweck MR, et al. Kinetic modelling and quantification bias in small animal PET studies with [18F]AB5186, a novel 18 kDa translocator protein radiotracer. PLoS One. 2019;14(5):e0217515.

22. Wakita K, Imahori Y, Ido T, Fujii R, Horii H, Shimizu M, et al. Simplification for measuring input function of FDG PET: investigation of 1-point blood sampling method. J Nucl Med. 2000;41(9):1484–90.

23. Vriens D, de Geus-Oei L-F, Oyen WJG, Visser EP. A curve-fitting approach to estimate the arterial plasma input function for the assessment of glucose metabolic rate and response to treatment. J Nucl Med. 2009;50(12):1933–9.

24. Tsuchida T, Sadato N, Yonekura Y, Nakamura S, Takahashi N, Sugimoto K, et al. Noninvasive measurement of cerebral metabolic rate of glucose using standardized input function. J Nucl Med. 1999;40(9):1441–5.

25. Takikawa S, Dhawan V, Spetsieris P, Robeson W, Chaly T, Dahl R, et al. Noninvasive quantitative fluorodeoxyglucose PET studies with an estimated input function derived from a population-based arterial blood curve. Radiology. 1993;188(1):131–6.

26. Takikawa S, Dhawan V, Chaly T, Robeson W, Dahl R, Zanzi I, et al. Input functions for 6-[fluorine-18]fluorodopa quantitation in parkinsonism: comparative studies and clinical correlations. J Nucl Med. 1994;35(6):955–63.

27. Mabrouk R, Strafella AP, Knezevic D, Ghadery C, Mizrahi R, Gharehgazlou A, et al. Feasibility study of TSPO quantification with [18F]FEPPA using population-based input function. PLoS One. 2017;12(5):e0177785.

28. Owen DRJ, Gunn RN, Rabiner EA, Bennacef I, Fujita M, Kreisl WC, et al. Mixed-affinity binding in humans with 18-kDa translocator protein ligands. J Nucl Med. 2011;52(1):24–32.

29. Owen DR, Guo Q, Kalk NJ, Colasanti A, Kalogiannopoulou D, Dimber R, et al. Determination of [(11)C]PBR28 binding potential in vivo: a first human TSPO blocking study. J Cereb Blood Flow Metab. 2014;34(6):989–94.

30. Hagens MHJ, Golla S V, Wijburg MT, Yaqub M, Heijtel D, Steenwijk MD, et al. In vivo assessment of neuroinflammation in progressive multiple sclerosis: a proof of concept study with F-18 DPA714 PET. J Neuroinflammation. 2018;15(1):314.

31. Coughlin JM, Wang Y, Ma S, Yue C, Kim PK, Adams A V, et al. Regional brain distribution of translocator protein using [11C]DPA-713 PET in individuals infected with HIV. J Neurovirol. 2014;20(3):219–32.

32. Wang Y, Coughlin J, Zhou Y, Ma S, Endres C, Pomper M. A method for personalized brain mapping of neuroinflammation using 11C-DPA-713 PET. J Nucl Med. 2013;54:529.

33. Vera JH, Guo Q, Cole JH, Boasso A, Greathead L, Kelleher P, et al. Neuroinflammation in treated HIV-positive individuals. Neurology. 2016;86(15):1425–32.

34. Jučaite A, Cselényi Z, Arvidsson A, Åhlberg G, Julin P, Varnäs K, et al. Kinetic analysis and test-retest variability of the radioligand [11C](R)-PK11195 binding to TSPO in the human brain - a PET study in control subjects. EJNMMI Res. 2012;2(1):15.

35. Fischl B. FreeSurfer. Neuroimage. 2012;62(2):774–81.

36. Herranz E, Giannì C, Louapre C, Treaba CA, Govindarajan ST, Ouellette R, et al. Neuroinflammatory

component of gray matter pathology in multiple sclerosis. Ann Neurol. 2016;80(5):776–90.

37. Bland JM, Altman DG. Statistical methods for assessing agreement between two methods of clinical measurement. Lancet. 1986;1(8476):307–10.

38. Schwartz J, Humm JL, Gonen M, Kalaigian H, Schoder H, Larson SM, et al. Repeatability of SUV measurements in serial PET. Med Phys. 2011;38(5):2629–38.

39. Karakatsanis N, Zhou Y, Lodge M, Casey M, Wahl R, Subramanian R, et al. Clinical Whole-body PET Patlak imaging 60-90min post-injection employing a population-based input function. J Nucl Med. 2015;56:1786.

40. Meyer PT, Circiumaru V, Cardi CA, Thomas DH, Bal H, Acton PD. Simplified quantification of small animal [18F]FDG PET studies using a standard arterial input function. Eur J Nucl Med Mol Imaging. 2006;33(8):948–54.

41. Arlicot N, Vercouillie J, Ribeiro MJ, Tauber C, Venel Y, Baulieu JL, et al. Initial evaluation in healthy humans of F-18 DPA-714, a potential PET biomarker for neuroinflammation. Nucl Med Biol. 2012;39(4):570–8.

42. Golla SS V, Boellaard R, Oikonen V, Hoffmann A, van Berckel BNM, Windhorst AD, et al. Quantification of F-18 DPA-714 binding in the human brain: initial studies in healthy controls and Alzheimer's disease patients. J Cereb Blood Flow Metab. 2015;35(5):766–72.

43. Ribeiro M-J, Vercouillie J, Debiais S, Cottier J-P, Bonnaud I, Camus V, et al. Could 18 F-DPA-714 PET imaging be interesting to use in the early post-stroke period? EJNMMI Res. 2014;4(1):28.

44. Hoekstra CJ, Hoekstra OS, Lammertsma AA. On the use of image-derived input functions in oncological fluorine-18 fluorodeoxyglucose positron emission tomography studies. Eur J Nucl Med. 1999;26(11):1489–92.

45. Drugan RC. Peripheral benzodiazepine receptors: molecular pharmacology to possible physiological significance in stress-induced hypertension. Clin Neuropharmacol. 1996;19(6):475–96.

46. Gavish M, Bachman I, Shoukrun R, Katz Y, Veenman L, Weisinger G, et al. Enigma of the peripheral

benzodiazepine receptor. Pharmacol Rev. 1999;51(4):629–50.

47. Ye Q, Lyu Z, Yao S, Dong Y, Liu H, Wu J, et al. Direct 4D Patlak Reconstruction in Dynamic FDG PET Imaging with Population-based Input Function. In: 2018 IEEE Nuclear Science Symposium and Medical Imaging Conference, NSS/MIC 2018 - Proceedings. 2018. p. 1–4.

Figures

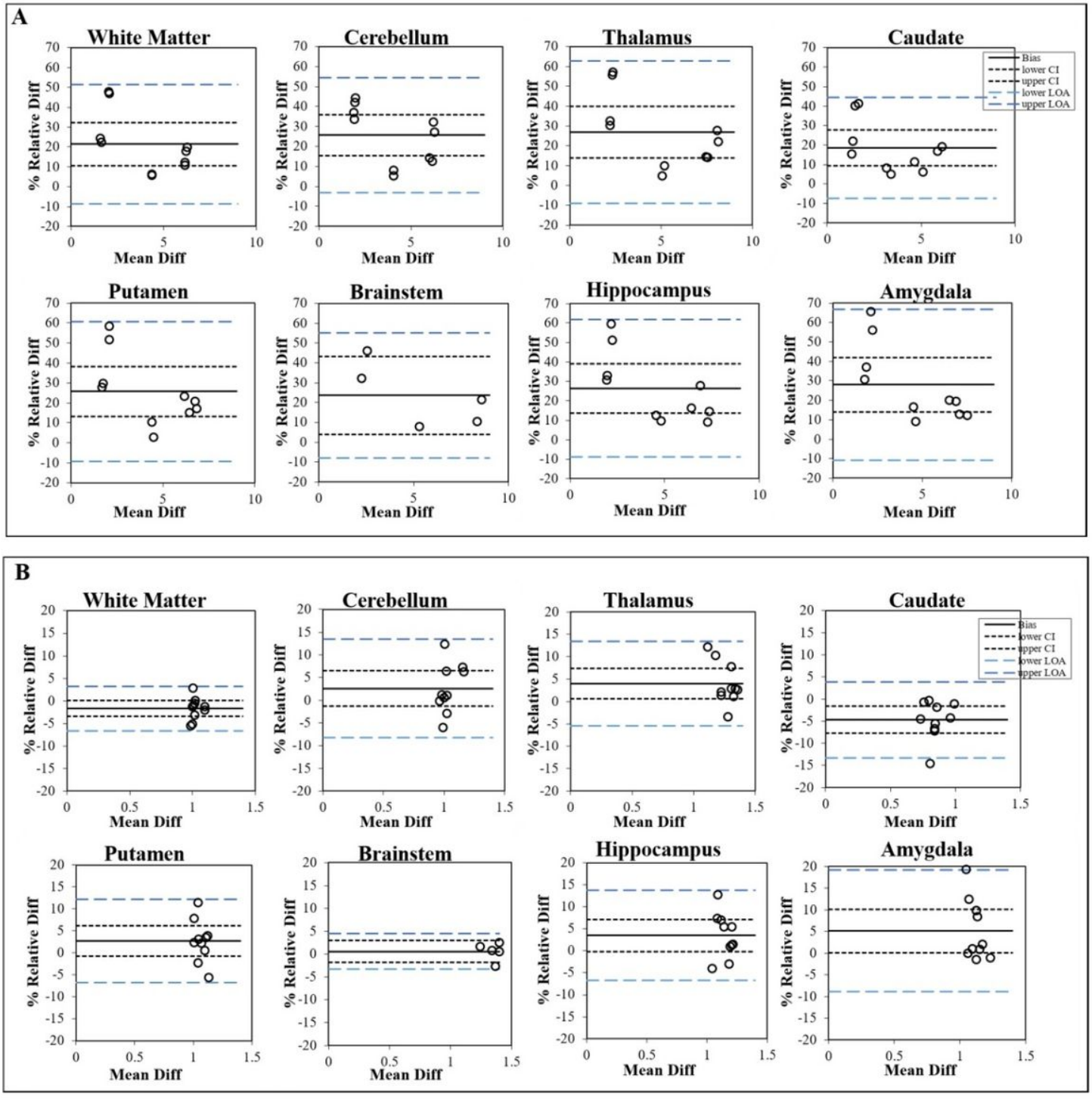

Figure 1

Bland-Altman plot comparing the test-retest repeatability of Vt estimates for all selected brain regions of interest: (A) without GM normalization and (B) with GM normalization respectively. The solid line is the mean % bias between test and retest VT estimate, while the doted and dashed lines represent the %CI and %LOA respectively

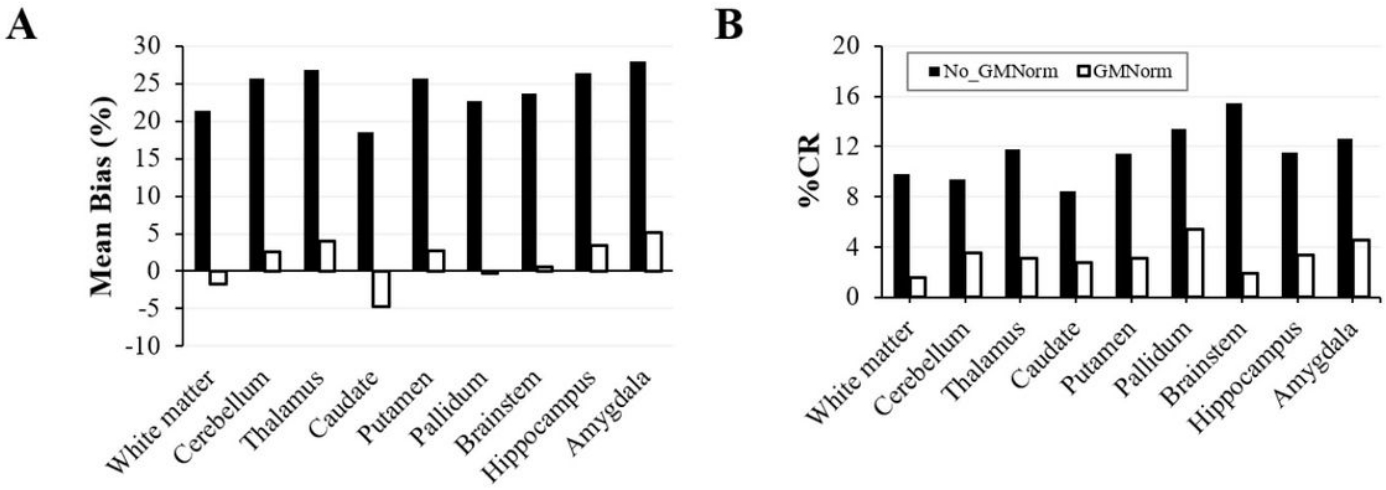

Figure 2

Effect of GM normalization on the (a) mean % bias and (b) CR of the test-retest VT estimate

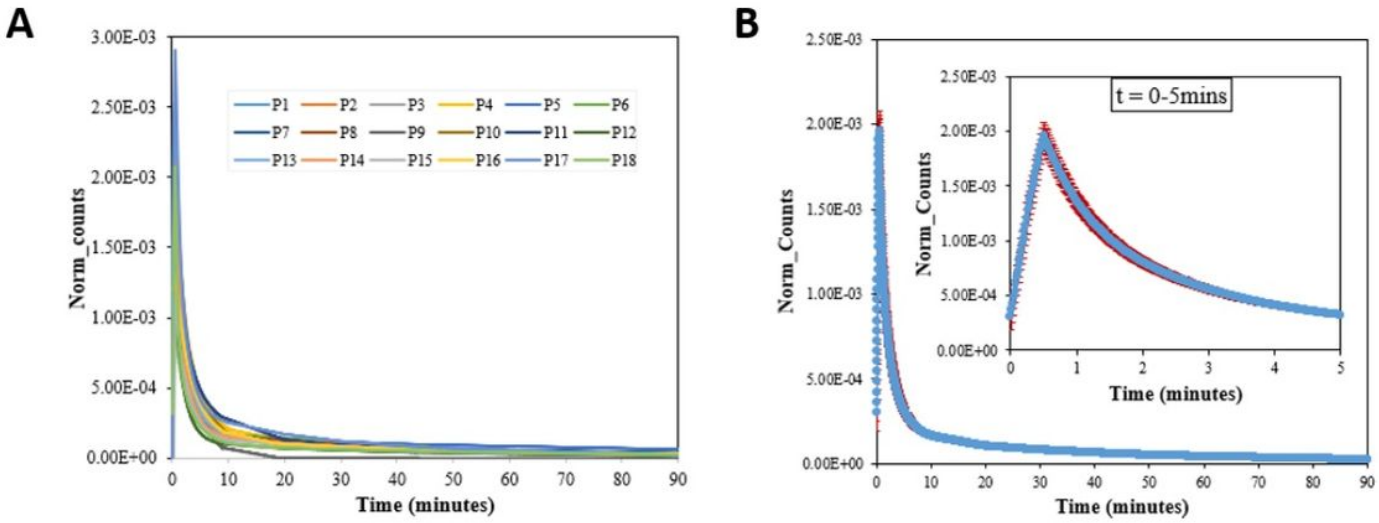

Figure 3

Overlaid normalized PSAIFs from all 18 patients (A) and the resulting PBIF generated by normalization with Weightsubject×AUC (B). The zoomed PBIF over the first 5 minutes is also shown. In (b), the blue points are the mean PBIF while the red points are the standard error of the mean (SEM)

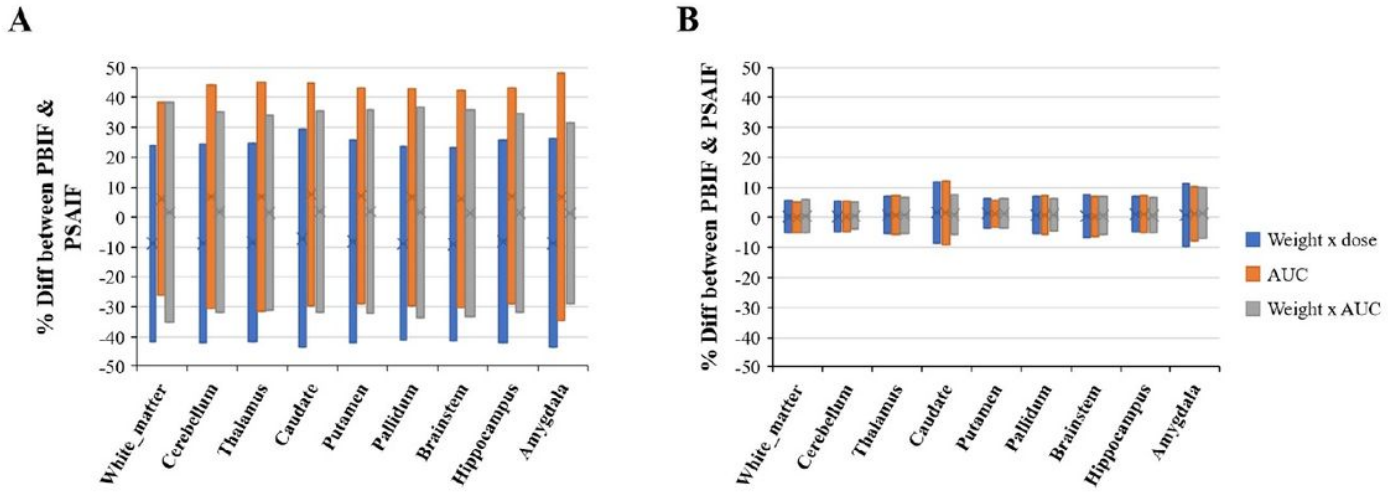

Figure 4

The % relative difference in VT and the LoAs between PSAIF and PBIF of some specific structures as generated by the three normalization techniques: (A) without GM normalization, (B) with GM normalization

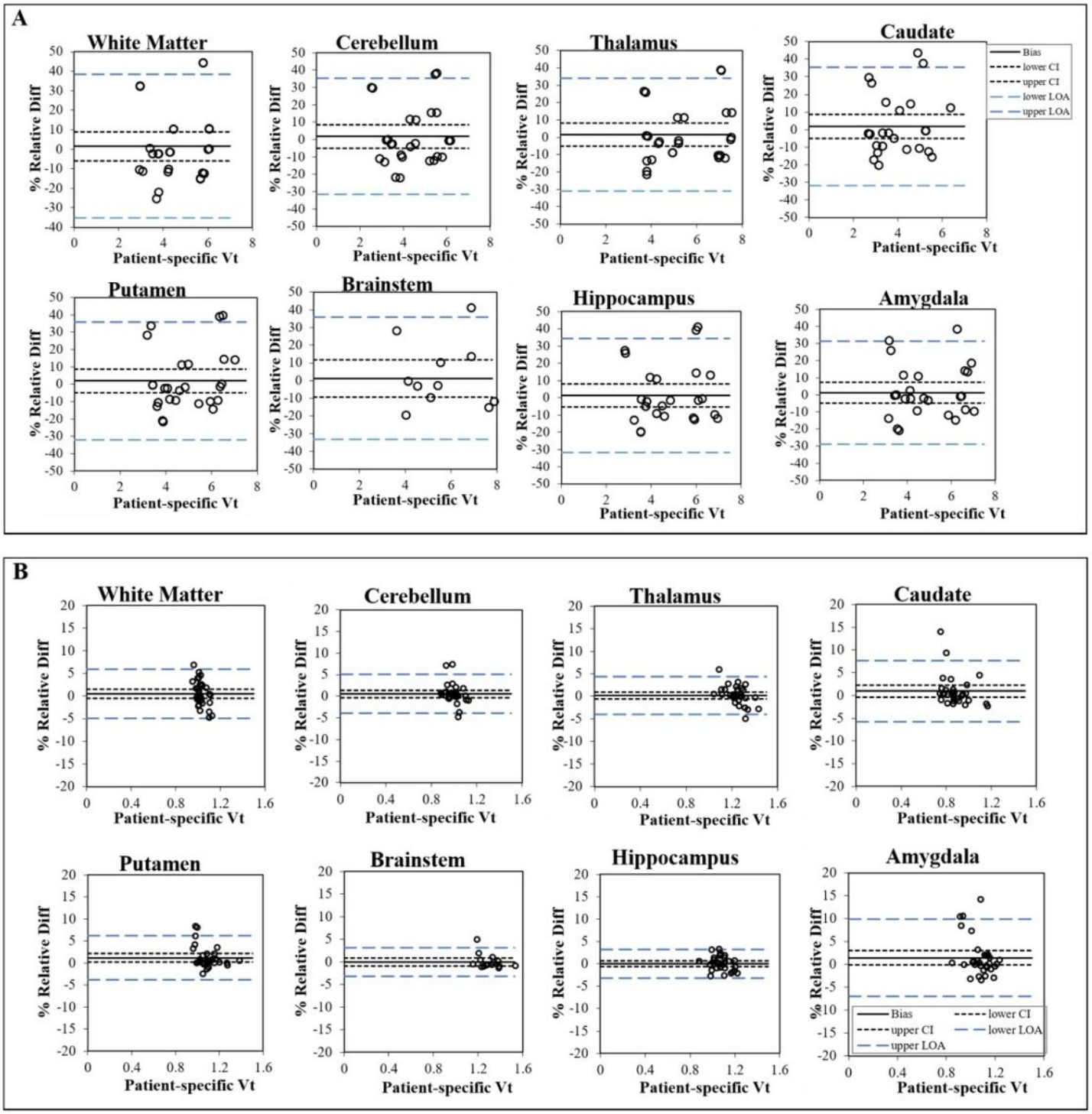

Figure 5

Bland-Altman analysis showing the variation in the VT between the PSAIF and PBIF (normalization with Weightsubject×AUC) with (A) no GM normalization and (B) GM normalization. The solid line is the mean % bias between PSAIF and PBIF VT estimate, while the doted and dashed lines represent the %CI and %LOA respectively